Dalton Transactions

ROYAL SOCIETY OF CHEMISTRY

PAPER

View Article Online
View Journal | View Issue

Check for updates

Cite this: *Dalton Trans.*, 2025, **54**, 12590

Fluoro- & trifluoromethoxy-modified bis(imino) pyridyliron chloride enhancing the activity and stability of vinyl polyethylenes†

Zahra Hosseinzadeh, [a] Qiuyue Zhang, [a] Jiahao Gao,[a] Yizhou Wang, [a,b] Quanchao Wang, [a,b] Geng Ren,[a] Tongling Liang, [a] Yanping Ma [a] and Wen-Hua Sun *[a,b]

The bis(imino)pyridylferrous chloride complexes bearing *para*-trifluoromethoxy and *ortho*-difluorobenzhydryl substituents, namely, 2-(1-{2,6-bis[bis(4-fluorophenyl)methyl]-4-trifluoromethoxyphenyl-imino} ethyl)-6-[1-(2,6-di(R^1)-4-R^2-phenylimino) ethyl]pyridyl iron(II) chloride (where R^1 = Me, R^2 = H, **Fe1**; R^1 = Et, R^2 = H, **Fe2**; R^1 = i-Pr, R^2 = H, **Fe3**; R^1 = Me, R^2 = Me, **Fe4**; R^1 = Et, R^2 = Me, **Fe5**; and R^1 = $(4\text{-}FC_6H_4)_2CH$, R^2 = OCF_3, **Fe6**) were successfully synthesized and thoroughly characterized. The X-ray crystal structures of **Fe4** and **Fe6** were also determined. The catalytic performance of all the new iron complexes was systematically evaluated for ethylene polymerization, with a detailed comparative analysis conducted against previously published studies. Notably, iron complexes **Fe1–Fe5** demonstrated exceptional catalytic activity and thermal stability upon activation with MAO, while **Fe6** showed inferior performance due to its significant steric hindrance. Among them, **Fe1** demonstrated the highest activity, achieving a peak of 17.28×10^6 g (PE) mol^{-1} (Fe) h^{-1} at 70 °C in *n*-hexane, which markedly surpassed the activity levels of other structurally related iron complexes, indicating the beneficial impact of incorporating multi-fluoro groups. Remarkably, the current iron pre-catalysts generally revealed superior performance in hexane compared to toluene, even when using a reduced quantity of co-catalyst, thereby underscoring the pivotal role of solvent polarity in governing the polymerization process. Furthermore, the analysis of the generated polyethylenes (PEs) revealed a high degree of linearity in the polymers, featuring vinyl end groups and exhibiting a broad spectrum of molecular weights (M_w: 4.5–567.9 kg mol^{-1}).

Received 8th April 2025,
Accepted 17th July 2025

DOI: 10.1039/d5dt00837a

rsc.li/dalton

Introduction

Polyethylene plays a central role in daily life and industrial applications due to its widespread use in the production of span films, insulated cables, piping systems, and engineering plastics.[1] Among the myriad carbon–carbon bond-forming reactions,[2] transition metal-catalyzed ethylene polymerization of ethylene holds a pivotal position in the chemical industry.[3] The advent of late transition metal catalysts in the mid-1990s marked a transformative breakthrough in polyolefin catalytic technology, building on the foundational developments with Ziegler–Natta catalysts in the 1950s and metallocene catalysts in the 1980s. In particular, tridentate bis(imino)pyridyl iron complexes (**A**, Chart 1) have emerged as highly efficient pre-catalysts, exhibiting remarkable performance in producing highly linear α-olefins/polyethylenes,[4] symbolizing a significant

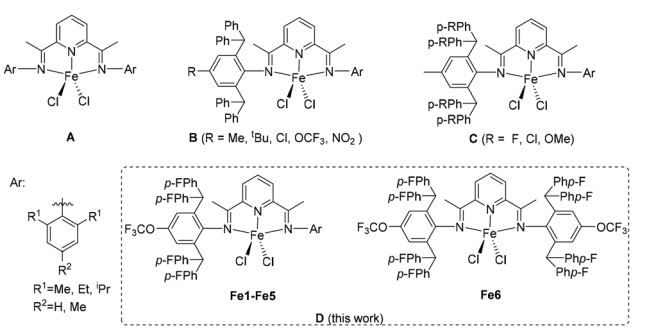

Chart 1 The classic bis(imino)pyridine-iron chloride **A**, along with its benzhydryl-substituted iron derivatives, **B–D**.

[a]*Key Laboratory of Engineering Plastics and Beijing National Laboratory for Molecular Sciences, Institute of Chemistry Chinese Academy of Sciences, Beijing 100190, China. E-mail: whsun@iccas.ac.cn*
[b]*CAS Research/Education Center for Excellence in Molecular Sciences, University of Chinese Academy of Sciences, Beijing 100049, China*

† Electronic supplementary information (ESI) available: GPC and DSC curves are collected as well as representative ^{13}C NMR of the resultant polyethylenes. Crystal data and structure refinement are provided for **Fe4** and **Fe6**. CCDC 2266904 and 2266905. For ESI and crystallographic data in CIF or other electronic format see DOI: https://doi.org/10.1039/d5dt00837a

achievement in the field of late transition metal catalysts for polyolefins. Subsequently, extensive research efforts have been directed toward modifying the bis(imino)pyridine backbone and *N*-aryl groups through the incorporation of diverse electronic and steric features, aiming to significantly enhance the catalytic proficiency of these systems.[5]

Previous studies have demonstrated that the presence of bulky substituents at the *ortho*-positions of the *N*-aryl groups significantly enhances the catalytic performance and thermal stability of the resulting complexes. In other words, the presence of bulky groups such as benzhydryl ($CHPh_2$) in iron complexes (**B**, Chart 1) not only remarkably generates higher molecular weight PEs by reducing the rate of chain transfer but also increases thermal stability and catalytic performance by shielding the apical positions of the metal centers.[6] Meanwhile, the electronic properties of *para*-substituents in the *N*-aryl groups can also influence the catalytic performance of catalysts by modulating the ligand structure and electron density around the central metal of the complex. Specifically, compared with complexes containing electron-donating groups, generally both the catalytic activity and the molecular weight of polyethylene produced by iron complexes with electron-withdrawing groups at the *para*-position of the *N*-aryl groups can be enhanced.[6] Nevertheless, excessive steric hindrance from the vertical side could significantly hinder ethylene coordination and insertion reactions, leading to drastically reduced activity.

Given the significant influence of the electronic effects of the ligand skeleton on the catalytic behavior of iron complexes, various remote substituents with distinct electronic properties (specifically, F, Cl, and OCH_3) have been introduced into the diphenylmethyl moiety to investigate how electronic modifications can modulate and enhance catalytic performance.[7] When the diphenylmethyl group was modified using electron-withdrawing *para*-fluoro or chloro substituents, the resulting iron complexes **C** (R = F and Cl, Chart 1) demonstrated enhanced catalytic activity, but led to the production of polyethylenes with lower molecular weights.[7a,b] Additionally, the thermal stability of another di(arylimine)pyridine iron(II) complex that incorporated a remote fluorine group within the *N*-2,6-di{di(4-fluorophenyl)methyl}-4-nitrophenyl group was significantly improved,[7d] compared to its fluorine-free iron analogues.[6e] For cobalt complexes, which typically exhibit lower performance in ethylene polymerization, significant improvements in both polymerization activity and thermal stability can be achieved by structural refinement through the incorporation of remote electron-withdrawing substituents, such as *para*-fluoride (F) or chloride (Cl) substituents.[5] Conversely, the introduction of an electron-donating *para*-methoxy group at the benzhydryl substituent into the iron complexes **C** (R = OCH_3, Chart 1) resulted in a notable increase in the polyethylene's molecular weight and a broadening of its molecular weight distribution, albeit at the expense of significantly diminished catalytic activity.[7c] In general, the electronic properties of the remote substituents on the benzhydryl groups significantly influenced the catalytic efficiency and thermal stability of bis(imino)pyridine-iron complexes, as well as the properties of the resulting polyethylenes, regardless of their distance from the iron center.

Inspired by a recently published series of ligands,[8] we synthesized a series of unsymmetrical bis(imino)pyridine-iron pre-catalysts (**D**, Chart 1) featuring one *N*-aryl group substituted with a *para*-trifluoromethoxy group (OCF_3) and two *ortho*-difluorobenzhydryl groups to gain a deeper understanding of the effects of electron-withdrawing groups on iron-catalyzed ethylene polymerization. This design allowed us to further investigate the beneficial role of remote fluoro groups and to assess the combined effects of the strong σ-inductive effect and minimal π-donating influence of the OCF_3 group.[9] Hexane, a widely used industrial solvent, was chosen as the polymerization medium to investigate its influence on the formation of active species and the polymerization process, with comparisons drawn to toluene.[6b] In order to investigate their catalytic behaviour thoroughly, polymerization reactions were conducted under various conditions, including ethylene pressure, polymerization time, polymerization temperature, co-catalyst type, and co-catalyst dosage, aimed at identifying optimal polymerization conditions and exploring how these factors influence the catalytic performance and properties of the resulting polyethylenes.

Results and discussion

Synthesis and identification of the ligands and iron complexes

A distinct set of unsymmetrically substituted ligands, 2-[CMeN{2,6-{$(4\text{-}FC_6H_4)_2CH$}$_2$-4-$OCF_3C_6H_2$}]-6-(CMeNAr)C_5H_3N (Ar = 2,6-$Me_2C_6H_3$, **L1**; 2,6-$Et_2C_6H_3$, **L2**; 2,6-i-$Pr_2C_6H_3$, **L3**; 2,4,6-$Me_3C_6H_2$, **L4**; 2,6-Et_2-4-MeC_6H_2, **L5**; 2,6-[$(4\text{-}F\text{-}C_6H_4)_2$]-4-$OCF_3$-$C_6H_2$, **L6**), has been synthesized through two consecutive Schiff base condensation reactions in our previous work (Scheme 1).[8] Subsequently, the iron complexes, [2-[CMeN{2,6-{$(FC_6H_4)_2CH$}$_2$-4-$OCF_3C_6H_2$}]-6-(CMeNAr)C_5H_3N]$FeCl_2$ (Ar = 2,6-$Me_2C_6H_3$, **Fe1**; 2,6-$Et_2C_6H_3$, **Fe2**; 2,6-i-$Pr_2C_6H_3$, **Fe3**; 2,4,6-$Me_3C_6H_2$, **Fe4**; 2,6-Et_2-4-MeC_6H_2, **Fe5**; 2,6-[$(4\text{-}F\text{-}C_6H_4)_2$]-4-$OCF_3$-$C_6H_2$ **Fe6**), were prepared by the stoichiometric reactions of iron dichloride with the respective ligands (**L1–L6**) in a blend of ethanol and dichloromethane under an inert nitrogen atmosphere at ambient temperature, achieving high yields ranging from 73% to 84% (Scheme 1). All newly synthesized iron complexes were identified by FT-IR, ^{19}F NMR spectroscopy and

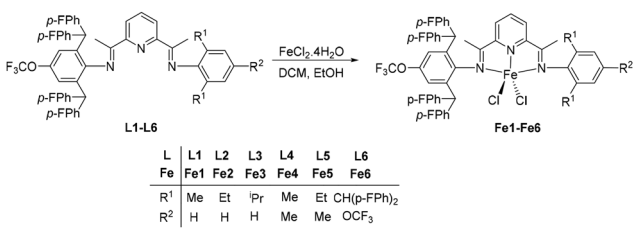

L	L1	L2	L3	L4	L5	L6
Fe	Fe1	Fe2	Fe3	Fe4	Fe5	Fe6
R^1	Me	Et	^{i}Pr	Me	Et	CH(p-FPh)$_2$
R^2	H	H	H	Me	Me	OCF_3

Scheme 1 The synthesis pathway for six iron(II) chloride complexes, **Fe1–Fe6**.

elemental analysis. Notably, the molecular structures of **Fe4** and **Fe6** were verified by single-crystal X-ray diffraction.

When comparing the ^{19}F NMR spectra of the ligands with those of their corresponding iron complexes, it was noted that the fluorine signals of the free ligands underwent a downfield shift, mirroring the trend observed in cobalt analogues.[8] Specifically, the $CH(4\text{-}FC_6H_4)_a(4\text{-}FC_6H_4)_b$ groups, which resided in distinct chemical environments, exhibited two non-equivalent fluorine groups within the range of −114.21 to −118.12 ppm. Conversely, the OCF_3 functional group comprised equivalent fluorine atoms, leading to a single peak within the range of −57.69 to −59.63 ppm (Fig. S1–S6†). Additionally, the IR spectra of the iron complexes exhibited a noticeable shift in the C=N stretching vibrations towards lower wavenumbers (1580–1605 cm^{-1}) compared to those observed in the free ligands (1600–1646 cm^{-1}), signifying the existence of a robust binding interaction between the imine-nitrogen atoms and the iron center.[10]

Two single crystals of iron complexes (**Fe4** and **Fe6**) were obtained by the slow diffusion of diethyl ether into their respective dichloromethane solutions under a nitrogen-protected atmosphere. The molecular structures of **Fe4** and **Fe6** are shown in Fig. 1 and 2, respectively, while the selected bond lengths and angles are shown in Table 1. Both **Fe4** and **Fe6** exhibit similar coordination structures that can be described as a distorted tetrahedral geometry, featuring a five-coordinate backbone where the iron center is coordinated by two chloride atoms and three nitrogen atoms from the 2,6-(bisarylimino) pyridine ligand.

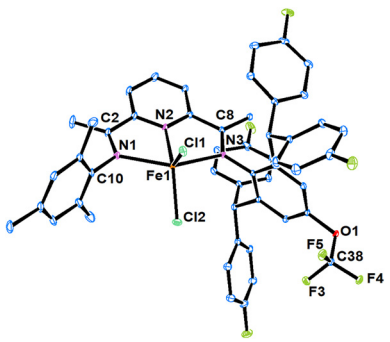

Fig. 1 Molecular structure of **Fe4** with the thermal ellipsoids shown at the 30% probability level; one molecule of dichloromethane and hydrogen atoms have been omitted for clarity.

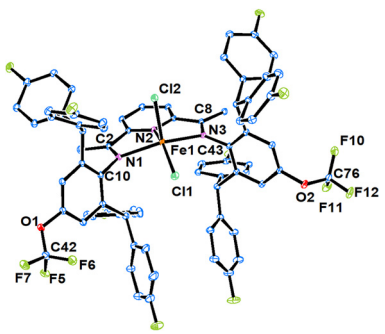

Fig. 2 Molecular structure of **Fe6** with the thermal ellipsoids shown at the 30% probability level; hydrogen atoms have been omitted for clarity.

Table 1 Selected bond lengths (Å) and angles (°) for **Fe4** and **Fe6**

	Fe4	Fe6
Bond lengths (Å)		
Fe(1)–N(1)	2.260(7)	2.2557(19)
Fe(1)–N(2)	2.114(7)	2.0748(19)
Fe(1)–N(3)	2.323(6)	2.2364(19)
Fe(1)–Cl(1)	2.289(3)	2.2380(7)
Fe(1)–Cl(2)	2.279(3)	2.3045(8)
N(1)–C(2)	1.282(12)	1.289(3)
N(1)–C(10)	1.431(10)	1.442(3)
N(2)–C(3)	1.362(10)	1.345(3)
N(2)–C(7)	1.337(10)	1.346(3)
N(3)–C(8)	1.296(10)	1.295(3)
N(3)–C(19)/C(43)	1.445(9)	1.436(3)
O(1)–C(38)/O(2)–C(76)	1.337(10)	1.324(4)
Bond angles (°)		
Cl(1)–Fe(1)–Cl(2)	108.52(12)	113.35(3)
N(1)–Fe(1)–N(2)	74.1(2)	73.19(7)
N(1)–Fe(1)–N(3)	146.1(2)	140.19(7)
N(1)–Fe(1)–Cl(1)	96.8(2)	99.45(5)
N(1)–Fe(1)–Cl(2)	105.0(2)	103.31(5)
N(2)–Fe(1)–N(3)	72.3(2)	73.35(7)
N(2)–Fe(1)–Cl(1)	118.4(2)	151.38(6)
N(2)–Fe(1)–Cl(2)	133.0(2)	95.26(6)
N(3)–Fe(1)–Cl(1)	102.76(18)	99.63(5)
N(3)–Fe(1)–Cl(2)	94.71(18)	100.62(5)

In the asymmetric structure of **Fe4**, the dihedral angles associated with the rings bonded to N(1) and N(3) are comparable (79.93° and 88.43°), indicating that the phenyl rings appended to the imine groups are nearly perpendicular to the coordination plane (Fig. 1). Regarding **Fe6**, it exhibits a configuration that closely approximates C_s symmetry, yet it is characterized by differing dihedral angles: specifically, 75.94° for the phenyl ring attached to N(1) and 83.84° for the phenyl ring attached to N(3). These discrepancies underscore the significant steric hindrance imparted by the benzhydryl substituents positioned on the *N*1-aryl group (Fig. 2). The iron atom exhibits distances of 0.125 Å and 0.570 Å to the plane formed by the coordinated nitrogen atoms (N1, N2, and N3) in **Fe4** and **Fe6**, respectively. Moreover, the central Fe–N2(Py) bond in **Fe4**, measuring 2.114(7) Å, is marginally elongated compared to the Fe–N2(Py) bond in **Fe6**, which spans 2.0748(19) Å. However, in both cases, the Fe–N2(Py) bonds are notably shorter than the Fe–N3(imine) bonds, which are 2.323(6) Å and 2.2364(19) Å, respectively, illustrating the robust coordination bond between the $N_{pyridine}$ atom and the central iron metal, as well as the pronounced axial influence exerted by large hindrance groups on the coordination center.[6e–f,7d] The bite angles N1–Fe–N2 and N2–Fe–N3 in **Fe6** are virtually identical, measuring 73.19(7)° and 73.35(7)° respectively. In contrast, the bite angles in **Fe4** exhibit a notable discrepancy, with values of 74.1(2)° and 72.3(2)°. This indicates that **Fe6** possesses a more symmetrical structure, whereas **Fe4** exhibits an unequal chemical environment around its iron center, attribu-

ted to the presence of two different *N*-aryl groups. However, the *ortho*-di(4-fluorophenyl)methyl substituents present in both *N*-aryl groups effectively obstruct the axial sites of the iron center in the symmetrical **Fe6** complex, thereby impeding the process of ethylene polymerization. The distance between the carbon atom and its neighboring oxygen atom in OCF_3, which measures 1.337(10) Å in **Fe4** and 1.324(4) Å in **Fe6**, reveals characteristics indicative of a double bond. This observation emphasizes the significant contribution of the ionic limiting resonance form $ArO^{+}{=}CF_2F^{-}$, akin to our previously reported findings.[6c,8]

Catalytic potential toward ethylene polymerization

To uncover the catalytic potential of the synthesized iron pre-catalysts **Fe1–Fe6**, polymerization experiments were conducted utilizing two distinct co-catalysts: methyl aluminoxane (MAO) and its modified counterpart, MMAO. Subsequently, the influence of the solvent was explored using the more potent co-catalyst. Prior to this, a systematic optimization process was undertaken, encompassing key polymerization parameters such as temperature, Al : Fe molar ratio, duration, and ethylene feed pressure. Upon establishing the optimal conditions, the remaining pre-catalysts (**Fe2–Fe6**) were evaluated for their efficacy in ethylene polymerization. The physical attributes of the resultant polyethylene (PE), including molecular weight (M_w) and melting point (T_m), were ascertained through gel permeation chromatography (GPC) and differential scanning calorimetry (DSC), respectively. Additionally, high-temperature $^1H/^{13}C$ NMR spectroscopy was employed to elucidate the microstructural characteristics of the obtained PE samples.

Catalytic evaluation of Fe1–Fe6/MAO in toluene

To refine the polymerization conditions, **Fe1** was selected as the test pre-catalyst and paired with MAO as the co-catalyst, and the polymerization results are detailed in Table 2. Initially, the influence of temperature on the catalytic performance was examined by varying the temperature between 40 and 100 °C with the Al : Fe molar ratio fixed at 2000 and a reaction run time of 30 min (runs 1–7, Table 2). These temperature adjustments revealed a significant impact on the catalytic properties and the resultant polyethylene (PE) properties. It was observed that **Fe1**/MAO exhibited lower catalytic activity at 40–50 °C but produced higher molecular weight PEs (198.7 to 567.9 kg mol^{-1}) (runs 1–2, Table 2), indicating a greater probability of chain propagation within this temperature range. As the temperature increased from 60 to 80 °C, the catalytic performance gradually improved, peaking at 14.23×10^6 g (PE) mol^{-1} (Fe) h^{-1} at 80 °C (runs 3–5, Table 2). When compared with the structurally related *N*-2,6-dibenzhydryl-4-trifluoromethoxyphenyl-containing $\mathbf{B_{OCF3}}$ (Chart 1),[6b] it is evident that the presence of the difluorobenzhydryl groups leads to an improvement in both the catalytic activity and thermal stability (optimal temp. 60 °C, 5.81×10^6 g (PE) mol^{-1} (Fe) h^{-1} for $\mathbf{B_{OCF3}}$ *vs.* optimal temp. 80 °C, 14.23×10^6 g (PE) mol^{-1} (Fe) h^{-1} for **Fe1**).

Above 80 °C, the catalytic performance declined slightly to 10.68×10^6 g (PE) mol^{-1} (Fe) h^{-1} at 90 °C (run 6, Table 2), potentially due to reduced monomer solubility or partial deactivation of the active species.[11,17] Despite the slight decrease at higher temperatures (above 90 °C), the catalytic performance remained robust at 2.5×10^6 g (PE) mol^{-1} (Fe) h^{-1}, out-

Table 2 Ethylene polymerization by **Fe1**–**Fe6**/MAO using toluene as the polymerization solvent[a]

Run	Pre-cat.	T (°C)	t (min)	Al : Fe	Act.[b]	M_w[c]	M_w/M_n[c]	T_m[d] (°C)
1	**Fe1**	40	30	2000	4.54	567.9	77.24	133.7
2	**Fe1**	50	30	2000	5.10	198.7	28.4	131.8
3	**Fe1**	60	30	2000	6.62	64.6	9.8	131.2
4	**Fe1**	70	30	2000	10.95	59.0	5.4	131.3
5	**Fe1**	80	30	2000	14.23	35.7	4.5	129.0
6	**Fe1**	90	30	2000	10.68	13.5	3.1	130.0
7	**Fe1**	100	30	2000	2.50	4.5	3.0	124.3
8	**Fe1**	80	30	1000	0.28	195.5	7.4	133.8
9	**Fe1**	80	30	1500	6.98	40.7	4.2	131.7
10	**Fe1**	80	30	2500	9.95	37.0	4.3	130.8
11	**Fe1**	80	30	2750	8.09	16.2	3.5	129.7
12	**Fe1**	80	30	3000	6.65	10.9	3.5	128.1
13	**Fe1**	80	05	2000	39.51	4.1	2.6	125.5
14	**Fe1**	80	15	2000	15.14	14.7	4.0	128.7
15	**Fe1**	80	45	2000	9.83	41.3	3.7	130.4
16	**Fe1**	80	60	2000	7.66	47.3	7.8	128.8
17[e]	**Fe1**	80	30	2000	6.12	9.4	4.5	126.1
18[f]	**Fe1**	80	30	2000	1.50	2.9	3.5	122.8
19	**Fe2**	80	30	2000	15.11	12.7	3.2	128.5
20	**Fe3**	80	30	2000	8.71	15.2	5.4	128.2
21	**Fe4**	80	30	2000	14.5	10.9	4.1	127.3
22	**Fe5**	80	30	2000	15.71	11.4	2.6	128.8
23	**Fe6**	80	30	2000	0.58	13.0	4.6	128.2

[a] Conditions: 2.0 μmol of **Fe** pre-catalyst, 100 mL toluene, 10 atm C_2H_4. [b] 10^6 g (PE) mol^{-1} (Fe) h^{-1}. [c] M_w (kg mol^{-1}), M_w and M_w/M_n determined by GPC. [d] Determined by DSC. [e] $P_{C_2H_4}$ = 5 atm. [f] $P_{C_2H_4}$ = 1 atm.

performing related pre-catalysts,[6e,7d] underscoring the high thermal stability of the current system. In contrast to the catalytic performance, the molecular weights of the produced PEs consistently decreased with the increase of reaction temperature (M_w: 567.9 to 4.5 kg mol^{-1}), likely due to a higher propensity for chain transfer compared to chain propagation.[6,11,12] Fig. S7† shows that the PEs exhibited broad molecular weight distributions at lower temperatures (40–70 °C), shifting to narrower distributions at higher temperatures (80–100 °C), indicating a transition towards single-site active species. Furthermore, the high melting temperatures, ranging from 125.5 to 133.8 °C, affirm the linear nature of the resulting PEs, which will undergo further analysis *via* high-temperature ^{1}H/^{13}C NMR in the sections that follow.

Secondly, the impact of varying the Al : Fe molar ratio within the range of 100 to 3000 was investigated while maintaining a constant temperature of 80 °C and a reaction time of 30 minutes (runs 5, 8–12, Table 2). Notably, at an Al : Fe molar ratio of 1000, the molecular weight of the resulting PEs reached a peak of 195.5 kg mol^{-1}, subsequently decreasing to 10.9 kg mol^{-1} as the ratio was increased to 3000. This observation could likely be attributed to the elevated concentrations of co-catalyst, which facilitated chain transfer from the iron active species to the aluminum center.[13] The optimal catalytic performance, achieving a rate of 14.23 × 10^6 g (PE) mol^{-1} (Fe) h^{-1}, was achieved at a 2000 Al : Fe molar ratio (run 5, Table 2). Consistent with previous observations, all polymers demonstrated a wide range of molecular weight distributions, exhibiting a general tendency towards narrowing as the quantity of co-catalyst utilized increased (Fig. S8†).

Third, to assess the longevity of **Fe1**/MAO, polymerization reactions were conducted over varying durations of 5, 15, 30, 45 and 60 minutes, with a reaction temperature of 80 °C and an Al : Fe molar ratio of 2000 (runs 5, 13–16, Table 2). Analysis of the results revealed a peak in catalytic performance at 5 min, achieving an activity level of 39.5 × 10^6 g (PE) mol^{-1} (Fe) h^{-1}. This surge in performance can be attributed to the rapid generation of numerous active species following the injection of MAO into the reaction mixture. Subsequently, the catalytic performance decreased steadily due to the partial deactivation of these active sites.[14] Despite this decline, a considerable performance of 7.66 × 10^6 g (PE) mol^{-1} (Fe) h^{-1} was maintained after 1 h of reaction, highlighting the impressive longevity of this pre-catalyst. With regard to the molecular weight of the resulting PEs, a gradual increase from 4.1 to 47.3 kg mol^{-1} was observed as the reaction time prolonged. This trend can be attributed to the persistence of sufficient active species over extended reaction periods (Fig. S9†).[15] The influence of ethylene pressure was also investigated under the optimized reaction conditions. As the ethylene pressure was reduced from 10 atm (run 5, Table 2) to 5 atm (run 17, Table 2) and then to 1 atm (run 18, Table 2), the catalytic performance decreased accordingly, from 14.23 to 6.12 × 10^6 g (PE) mol^{-1} (Fe) h^{-1} and then to 1.5 × 10^6 g (PE) mol^{-1} (Fe) h^{-1}. Similarly, the molecular weights of PEs decreased from 35.7 kg mol^{-1} to 9.4 kg mol^{-1} and then to 2.9 kg mol^{-1}, indicating a close correlation between the coordination and insertion rate of ethylene and the concentration of ethylene supplied.[7]

Finally, to explore the electronic and steric effects on catalytic performance, the remaining pre-catalysts (**Fe2–Fe6**) were evaluated under the optimized conditions [Al : Fe = 2000, 80 °C, 30 minutes, 10 atm] (runs 19–23, Table 2). All iron pre-catalysts except **Fe6**, which possessed the largest steric hindrance, exhibited high catalytic performance ranging from 8.71 to 15.71 × 10^6 g (PE) mol^{-1} (Fe) h^{-1}, and the activity trend was listed as follows: **Fe5** > **Fe2** > **Fe4** > **Fe1** > **Fe3** ≫ **Fe6**. In comparison with previously reported results obtained with the iron precatalyst $\mathbf{B_{OCF3}}$ (Chart 1),[6b] the current iron systems gave improved activity even at higher polymerization temperatures [(3.61–9.66) × 10^6 g (PE) mol^{-1} (Fe) h^{-1} for $\mathbf{B_{OCF3}}$ at 60 °C *vs.* (8.71–15.71) × 10^6 g (PE) mol^{-1} (Fe) h^{-1} for **D** at 80 °C], highlighting the better thermal stability and catalytic efficacy of the current catalysts containing remote fluoro-substituents. The presence of substantial steric hindrance at the *ortho*-position in **Fe3** and **Fe6** could impede the seamless incorporation of the ethylene monomer and retard the transfer of iron active species along the chain, ultimately resulting in diminished catalytic efficiency and the generation of polyethylenes with increased molecular weights.[6a,d,e,16] Moreover, **Fe4** and **Fe5** bearing electron-donating methyl groups at the *para*-position of the *N*-aryl ring exhibited superior activities compared to their counterparts **Fe1** and **Fe2**, respectively, consistent with previous observations for iron pre-catalysts.[6d,e] In general, much lower molecular weight PEs were obtained by **Fe1–Fe6** (M_w: 10.9–35.7 kg mol^{-1}) (Fig. S10†) in comparison with those obtained from structurally related iron pre-catalysts (**B** and **C**, Chart 1), indicating that the introduction of remote electron-withdrawing substituents had a significant impact on chain transfer from the active centers.[6,7] Notably, all the resulting PEs exhibited unimodal molecular weight distributions, coupled with high melting points, indicating their linear nature as well as the uniform active species during the polymerization process. Within the current reaction setup, the deactivation of the active species tended to occur as the temperature rose or the reaction proceeded for a longer period. The root causes are that the iron active species undergoes easier redox deactivation upon binding with impurities (*e.g.*, aluminum alkyls) and the inactive species may form due to structural changes (*e.g.*, ligand dissociation and dimerization) and β-H elimination, which effectively removes it from the polymerization cycle.

Catalytic evaluation of Fe1–Fe6/MAO in hexane

To investigate the influence of the polymerization solvent on catalytic performance, experiments were conducted using hexane as the solvent. In a manner similar to that described for **Fe**/MAO in toluene, the polymerization conditions in hexane were again optimized by employing **Fe1** as the test pre-catalyst. Meanwhile, the catalytic activities of **Fe1–Fe6** and the properties of the resulting polyethylenes (PEs) were evaluated, with the results summarized in Table 3.

Table 3 Ethylene polymerization by **Fe1–Fe6**/MAO using *n*-hexane as the solvent[a]

Run	Pre-cat.	T (°C)	t (min)	Al : Fe	Act.[b]	M_w[c]	M_w/M_n[c]	T_m[d] (°C)
1	**Fe1**	50	30	1500	6.23	411.3	39.2	133.0
2	**Fe1**	60	30	1500	9.31	354.6	59.8	131.9
3	**Fe1**	70	30	1500	12.52	56.4	11.0	129.6
4	**Fe1**	80	30	1500	10.20	7.8	2.5	126.8
5	**Fe1**	70	30	500	8.36	267.4	19.9	133.4
6	**Fe1**	70	30	750	13.84	148.9	12.0	132.9
7	**Fe1**	70	30	1000	17.28	134.4	12.5	132.4
8	**Fe1**	70	30	1250	12.97	88.7	10.1	132.0
9	**Fe2**	70	30	1000	13.80	177.3	24.0	132.3
10	**Fe3**	70	30	1000	10.45	290.2	34.9	132.5
11	**Fe4**	70	30	1000	16.12	143.0	18.2	132.7
12	**Fe5**	70	30	1000	13.58	227.9	34.3	131.6
13	**Fe6**	70	30	1000	0.50	178.2	61.7	131.3

[a] Conditions: 2.0 μmol of **Fe** pre-catalyst, 100 mL of hexane, 10 atm C_2H_4. [b] 10^6 g (PE) mol^{-1} (Fe) h^{-1}. [c] M_w (kg mol^{-1}), M_w and M_w/M_n determined by GPC. [d] Determined by DSC.

Initially, the thermal stability of the **Fe1**/MAO system was assessed between 50 °C and 80 °C with an Al : Fe molar ratio of 1500 : 1 in hexane under 10 atm of C_2H_4 (runs 1–4, Table 3). The best activity of 12.52×10^6 g (PE) mol^{-1} (Fe) h^{-1} was again achieved at 70 °C, exceeding the performance observed in toluene at the same temperature (run 4, Table 2), indicating that the **Fe1**/MAO system exhibited better heat resistance *r* in *n*-hexane. GPC analysis (Fig. S11†) showed a trend similar to that in toluene, with higher molecular weight PEs (354.6–411.3 kg mol^{-1}) produced at lower temperatures. The bimodal polyethylenes obtained at low temperatures (50–60 °C) could be attributed to the multiple active species generated by residual alkyl aluminum in MAO, while the polyethylenes with the lowest molecular weight of 7.8 kg mol^{-1} produced at 80 °C exhibited the narrowest distribution, indicating the failure of unstable active species at high temperatures (run 4, Table 3).[11] In most cases, the resultant polyethylenes obtained in *n*-hexane had much wider polydispersities than those obtained in toluene, partly due to the low solubility of iron complexes in *n*-hexane.[4e]

Next, with the temperature held at 70 °C, the Al : Fe molar ratio was varied from 500 : 1 to 1500 : 1 (runs 3, 5–8, Table 3). Remarkably, an Al : Fe molar ratio of 1000 yielded the peak performance value of 17.28×10^6 g (PE) mol^{-1} (Fe) h^{-1} (run 7, Table 3). The optimal dosage of MAO for the catalytic system in hexane was significantly lower compared to the amounts typically utilized in toluene, emphasizing the economic viability of the current system and its applicability for industrial applications. However, no comparable enhancement was noted in the analogous system employing $\mathbf{B_{OCF3}}$ (Chart 1), despite the use of an even greater quantity of cocatalyst to activate the corresponding iron complexes.[7b]

Under the above optimized conditions in *n*-hexane, the remaining five iron pre-catalysts (**Fe2–Fe6**) were tested toward ethylene polymerization (runs 7, 9–13, Table 3). All six iron complexes revealed moderate or good catalytic activity ($(0.50–17.28) \times 10^6$ g (PE) mol^{-1} (Fe) h^{-1}), yielding high molecular weight polyethylenes (134.4–290.2 kg mol^{-1}) with broad molecular weight distributions (M_w/M_n: 12.5–61.7). The overall catalytic performances followed the order: **Fe1** > **Fe4** > **Fe2** > **Fe5** > **Fe3** ≫ **Fe6**. In terms of steric hindrance, **Fe6** and **Fe3**, which had the most significant steric hindrance, were the least active systems, whereas **Fe1** and **Fe4**, with the least steric hindrance, were the most active. Unlike the **Fe**/MAO system in toluene, the electronic properties of a *para*-methyl group on the *N*-aryl had no obvious positive effect on the catalytic performance.[13c,16] As illustrated in Fig. S13,† the molecular weight distributions of the resulting PEs exhibited a notable range, spanning from distinctly bimodal (**Fe2**, **Fe3**, **Fe5**, **Fe6**) to apparently unimodal (**Fe1**, **Fe4**). This variation underscores the differing proportions of two active species, which arise from distinct termination kinetics. The relative abundance of these species is, to some extent, influenced by the varying configurations of the active species, a consequence of the steric hindrance imposed by *ortho*-substituents.[4e] Generally, these iron pre-catalysts demonstrated superior activities and delivered polyethylenes with higher molecular weights in hexane compared to toluene.

Catalytic evaluation of Fe1–Fe6/MMAO in toluene

To investigate the impact of co-catalyst type on catalytic performance, MMAO was employed as an additional primary co-catalyst to activate these iron complexes for the purpose of ethylene polymerization in toluene; the polymerization data are summarized in Table 4.

When adjusting the temperature within the range of 50 to 90 °C (runs 1–5, Table 4) and modifying the Al : Fe molar ratio

Table 4 Ethylene polymerization by **Fe1–Fe6**/MMAO using toluene as the polymerization solvent[a]

Run	Pre-cat.	T (°C)	t (min)	Al/Fe	Act.[b]	M_w[c]	M_w/M_n[c]	T_m[d] (°C)
1	**Fe1**	50	30	2000	6.50	25.5	10.8	128.1
2	**Fe1**	60	30	2000	12.99	20.8	5.1	127.9
3	**Fe1**	70	30	2000	13.31	17.7	4.0	129.5
4	**Fe1**	80	30	2000	8.90	9.2	2.8	128.0
5	**Fe1**	90	30	2000	2.63	3.7	2.5	123.3
6	**Fe1**	70	30	1000	4.90	48.2	4.9	131.3
7	**Fe1**	70	30	1500	7.80	18.2	3.2	130.5
8	**Fe1**	70	30	2500	12.11	9.2	3.3	127.9
9	**Fe1**	70	30	3000	8.66	8.6	3.2	126.5
10	**Fe1**	70	05	2000	24.18	3.3	2.2	123.0
11	**Fe1**	70	15	2000	9.08	4.5	2.5	124.5
12	**Fe1**	70	45	2000	9.46	20.3	14.3	124.6
13	**Fe1**	70	60	2000	7.16	22.9	10.7	125.6
14[e]	**Fe1**	70	30	2000	2.40	1.5	1.5	119.8
15[f]	**Fe1**	70	30	2000	0.70	1.1	1.6	115.6
16	**Fe2**	70	30	2000	6.88	3.8	2.7	123.3
17	**Fe3**	70	30	2000	5.39	4.2	3.0	123.8
18	**Fe4**	70	30	2000	7.38	3.6	2.4	123.2
19	**Fe5**	70	30	2000	6.22	4.2	2.5	123.8
20	**Fe6**	70	30	2000	0.30	2.0	2.1	123.8

[a] Conditions: 2.0 μmol **Fe**, 100 mL toluene, 10 atm of C_2H_4. [b] 10^6 g of (PE) mol^{-1} (Fe) h^{-1}. [c] M_w: kg mol^{-1}, determined by GPC. [d] Determined by DSC. [e] 5 atm of C_2H_4. [f] 1 atm of C_2H_4.

from 1000 : 1 to 3000 : 1 (runs 3, 6–9, Table 4), a peak activity of 13.31 × 10^6 g (PE) mol^{-1} (Fe) h^{-1} was attained at 70 °C with an Al : Fe molar ratio of 2000 over a duration of 30 minutes. Analysis of the polymerization temperature-related data revealed that **Fe1**/MMAO exhibited inferior thermal stability compared to **Fe1**/MAO, producing PEs with decreased molecular weights and narrower molecular weight distributions (Fig. S14†).[6e,11] Furthermore, the Al : Fe molar ratio played a pivotal role in regulating the catalytic performance of iron complexes. As the Al : Fe molar ratio increased to 3000, the catalytic activity gradually declined from 13.31 × 10^6 g (PE) mol^{-1} (Fe) h^{-1} to 8.66 × 10^6 g (PE) mol^{-1} (Fe) h^{-1}, accompanied by a reduction in molecular weight from 48.2 kg mol^{-1} to 8.6 kg mol^{-1}, suggesting an elevated rate of chain transfer from active iron species to aluminum (Fig. S15†).[7] As the reaction time extended from 5 to 60 min, the catalytic activity decreased from 24.18 × 10^6 to 7.16 × 10^6 g (PE) mol^{-1} (Fe) h^{-1}, whereas the molecular weight of polyethylenes increased from 3.3 to 22.9 kg mol^{-1} (Fig. S16†), indicating a rapid generation of active species upon the addition of MMAO and a long lifetime of these pre-catalysts despite partial deactivation (runs 3, 10–13, Table 4). Additionally, the ethylene pressure was found to be directly proportional to both the activity and molecular weight of the resulting polymer, showing that a specific monomer concentration is a necessary condition for overcoming mass transport limitations (runs 3, 14 and 15, Table 4). When compared to the **Fe**/MAO system, **Fe1**–**Fe5**/MMAO exhibited considerably lower activities and generated polyethylenes with decreased molecular weights and narrower molecular weight distributions, with the exception of **Fe6**/MMAO (Fig. S17†). As previously observed, reducing steric hindrance at the *ortho*-aryl position and replacing the *para*-aryl proton with a methyl group can enhance catalytic performance.[6f,15,17a]

A comparative view of the previously reported and current iron pre-catalysts

To gain insights into how the structural enhancements achieved through the incorporation of *ortho*-difluorobenzhydryl and *p*-trifluoromethoxy groups influence the catalytic performance of iron pre-catalysts, a meticulous comparison of the performance attributes of the current precatalyst family (**D**, Chart 1) with previously documented **B** and **C** (Chart 1)[6a,b,f,7b–d] was conducted and is summarized in Fig. 3. The activity levels and optimal operating temperatures of **Fe4**, in particular, are presented alongside corresponding data of the mesityl-containing instances of **B** and **C**. All catalytic reactions were executed under conditions of 10 atm of C_2H_4, utilizing MAO as the activator.

In terms of catalytic activity, **Fe4** (**D**, Fig. 3) and $\mathbf{C_{Cl}}$[7b] emerged as notably more potent than other iron complexes, with **Fe4** achieving a peak activity of 15.71 × 10^6 g (PE) mol^{-1} (Fe) h^{-1} at 80 °C. Among all iron analogues, **Fe4** exhibited the highest optimal temperature (80 °C), highlighting the beneficial effects of incorporating multiple-fluoro-substituents into the precatalyst structure on both catalytic activity and thermal stability. Regarding the molecular weight of the resulting polyethylenes, the inclusion of a remote electron-donating group within the benzhydryl framework had a favorable effect, with the methoxy-containing $\mathbf{C_{OMe}}$[7c] yielding polymers of the highest molecular weight. This finding illustrates the capacity of the remote methoxy group to positively influence molecular weight within this set. Conversely, **Fe4** (**D**, Fig. 3) and $\mathbf{C_{Cl}}$,[7b] which contain electron-withdrawing substituents in their benzhydryl groups, exhibited the lowest molecular weight value (around 10.9 kg mol^{-1}), indicating the detrimental effects of electron-withdrawing groups on polymer chain growth. Due to the combined electronic effects of the remote substituents on benzhydryl and the *para*-substituents, **Fe4** (**D**, Fig. 3) exhibited a greater similarity to its chloride counterpart, $\mathbf{C_{Cl}}$,[7b] than to $\mathbf{C_F}$.[7a] Notably, the introduction of a remote fluoro group significantly boosted activity and led to the formation of a distinct type of polyethylene when compared to other trimethoxy-containing iron complexes, $\mathbf{B_{OCF3}}$.[6b] Furthermore, a comparative analysis between the previously documented cobalt analogues[8] and the present iron complexes reveals that the iron complexes demonstrate markedly superior thermal stability and yield polyethylenes characterized by broader molecular weight distributions. These findings strongly highlight the predominant advantages that iron complexes hold in facilitating efficient ethylene polymerization.

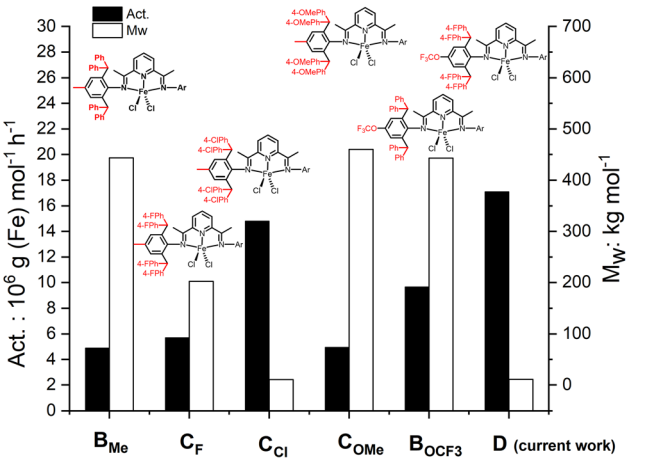

Fig. 3 Comparative catalytic performance of D (**Fe4** in this work) with mesityl-containing B_{Me}, C_F, C_{Cl}, C_{OMe} and B_{OCF3}; all runs were conducted with MAO as the activator under optimum conditions.

Microstructural properties of the resultant polyethylenes

All polyethylenes produced in this study exhibited high melting temperatures (≥126 °C), irrespective of the solvent or co-catalyst variations, indicating their high linearity.[18] Notably, only the samples produced at low pressure (*i.e.* 1 atm C_2H_4, run 18, Table 2) displayed melting temperatures below 126 °C. To further confirm the linearity and elucidate the end group configuration of these polyethylenes, high-temperature ^1H and ^{13}C NMR spectroscopy was performed on several selected samples: $PE_{\mathbf{Fe1}/MAO/toluene}$ (run 5, Table 2, M_w = 35.7 kg mol^{-1}),

$PE_{Fe1/MAO/hexane}$ (run 7, Table 3, M_w = 134.4 kg mol^{-1}), and $PE_{Fe1/MMAO/toluene}$ (run 3, Table 4, M_w = 17.7 kg mol^{-1}). For adequate solubility, the polyethylenes were pre-dissolved in 1,1,2,2-tetrachloroethane-d_2 at 100 °C, and the spectra were recorded at the same temperature.

For the typical sample $PE_{Fe1/MAO/toluene}$ (run 4, Table 2, M_w = 59.0 kg mol^{-1}), the presence of an intense signal at δ 1.30 in the ^{1}H NMR spectrum and δ 29.41 in the ^{13}C NMR spectrum served as evidence of the polyethylenes' linearity (Fig. 4). Moreover, the ^{1}H NMR spectrum revealed proton signals attributable to a vinyl group at δ 5.89 (H_b), δ 4.93 (H_a) and δ 4.99 (H_a') in a 1 : 1 : 1 ratio. The existence of two vinylic carbon signals at δ 115.87 (a) and δ 141.69 (b) in the ^{13}C NMR spectrum further supported this finding. Additionally, the ratio of the vinylic H_b proton to the methyl H_g protons at the opposite end of the PE chain was approximately 1 : 3, providing strong evidence for the presence of an unsaturated chain end. The vinylic H_b proton, indicative of a terminal double bond, suggested the presence of vinyl functionality at one end of the polyethylenes, while the methyl H_g protons confirmed a saturated structure at the other end. The ^{13}C NMR spectrum also provided clear evidence for the existence of a saturated chain end in the structure of polyethylenes, with distinct signals at δ 22.44 (f), corresponding to the methylene carbon and δ 13.85 (g) associated with the methyl end-group. These observations were consistent with the expected polymerization mechanism, where chain termination occurs through β-hydride elimination, leaving a vinyl group at the terminal position.[7] Importantly, identical signal integration and chemical shift assignments were also observed in other polyethylenes, namely, $PE_{Fe1/MMAO/toluene}$ and $PE_{Fe1/MAO/hexane}$, produced using different co-catalysts or polymerization solvents (Fig. S18–S20†), providing further evidence for the mechanistic reliability of the current catalytic systems. Interestingly, an analysis of the NMR spectra of polyethylene (PE) samples produced in hexane, with MAO serving as the co-catalyst, revealed the presence of an analogous vinyl chain-terminated group. This observation suggests that the polymerization solvent exerts a relatively minor influence on the chain termination mechanisms during the polymerization process. Meanwhile, the ^{13}C NMR spectrum of $PE_{Fe1/MMAO/toluene}$ exhibits several weak signals at chemical shifts, δ 39.12 (c), 27.93 (b), 27.30 (d) and 22.56 (a), which can be ascribed to an isobutyl end group, implying that both chain transfer to aluminum and β-H elimination served as viable chain termination pathways with β-H elimination being the predominant mechanism.

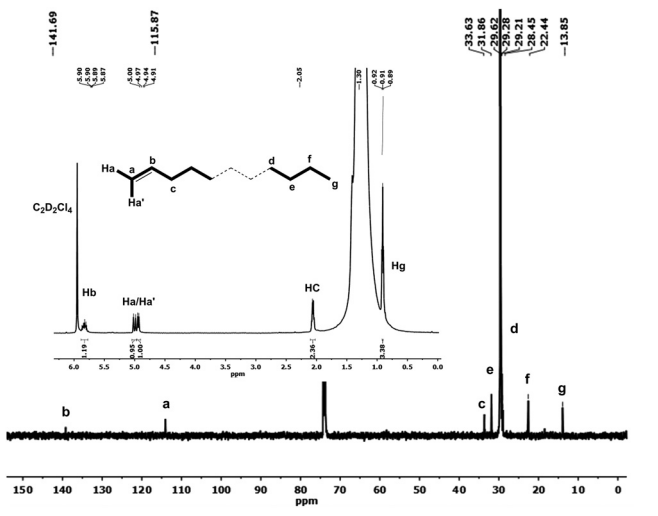

Fig. 4 The high temperature ^{13}C NMR spectrum of $PE_{Fe1/MAO/toluene}$ (run 5, Table 2) along with an inset of its high temperature ^{1}H NMR spectrum recorded in 1,1,2,2-tetrachloroethane-d_2 at 100 °C.

Experimental

General methods

To handle chemicals sensitive to air or moisture, standard Schlenk techniques were employed under an atmosphere of dry nitrogen or within a nitrogen-filled glove box. Prior to use, the solvents hexane and toluene were dried over sodium and distilled under nitrogen. Methylaluminoxane (1.46 M solution in toluene) and modified methylaluminoxane (1.93 M solution in *n*-heptane) were sourced from Anhui Botai Electronic Materials Co., while high-purity ethylene, obtained from Beijing Yanshan Petrochemical Corp., was used without further purification. Additional reagents were supplied by Aldrich, Acros, or local providers. The aniline, 2,6-bis(bis(4-fluorophenyl)methyl)-4-(trifluoromethoxy)aniline,[19] 2-acetyl-6-[1-(2,6-bis(bis(4-fluorophenyl)methyl)-4-trifluoromethoxyphenylimino)ethyl] pyridine (**A**) and the organic ligands (**L1–L6**)[8] were synthesized based on our previously published methods. FT-IR spectra were recorded using a PerkinElmer System 2000 FT-IR spectrometer, while elemental analyses were conducted on a Flash EA 1112 microanalyzer. ^{1}H and ^{13}C NMR spectra of all novel organic and inorganic compounds were obtained on a Bruker Avance 400 MHz spectrometer at room temperature, employing $CDCl_3$ as the solvent and TMS as the internal standard. ^{19}F NMR spectra were measured on a Bruker AVANCE 700 MHz instrument at ambient temperature. The melting temperatures (T_m) of the polyethylene (PE) samples were determined using a PerkinElmer TA-Q2000 DSC analyzer under a nitrogen atmosphere. The method involved heating a weighed sample (4.0–6.0 mg) to 160 °C at a rate of 20 °C min^{-1}, holding at 160 °C for 5 minutes to eliminate thermal history, and then cooling to −20 °C at a rate of 20 °C min^{-1}. Finally, the sample was heated to 160 °C at a rate of 10 °C min^{-1}. Gel permeation chromatography (GPC) of the PEs was performed using an Agilent PLGPC 220 instrument equipped with a refractive index (RI) detector operating at 160 °C, with 1,2,4-trichlorobenzene as the eluent. For the ^{1}H and ^{13}C NMR spectroscopy of the PEs, a weighed amount of PE (20–40 mg) was first dissolved in 1,1,2,2-tetrachloroethane-d_2 (1 mL) at elevated temperature, using TMS as the internal standard. The spectra were then recorded on a Bruker AVANCE III 500 MHz instrument at 100 °C. The operating conditions for the ^{1}H NMR spectra

included a spectral width of 15.000 kHz, an acquisition time of 2.1845 s, a relaxation delay of 2.0 s, and 64 scans. For the ^{13}C NMR spectra, the conditions were a spectral width of 31.250 kHz, an acquisition time of 0.52 s, a relaxation delay of 1.5 s, and 1024 scans.

Synthesis and characterization

Synthesis of [2-[CMeN{2,6-{(4-FC$_6$H$_4$)$_2$CH}$_2$-4-OCF$_3$}]-6-(CMeNAr)C$_5$H$_3$N]FeCl$_2$. Ar = 2,6-Me$_2$C$_6$H$_3$ (**Fe1**): Under a nitrogen atmosphere, a mixture comprising **L1** (0.27 mmol, 0.21 g) and $FeCl_2$ (0.27 mmol, 0.03 g) in a solvent blend of dichloromethane (10 mL) and ethanol (5 mL) was stirred at room temperature overnight. Subsequently, all volatiles were then removed under reduced pressure to give a concentrated solution. To precipitate the product, an excess of diethylether was introduced, and the resulting precipitate was collected *via* filtration and washed with diethylether (3 × 10 mL), yielding **Fe1** as a blue powder (0.21 g, 84%). FT-IR (cm^{-1}): 2970 (w), 2917 (W), 1628 (w), 1595 (C═N, m), 1505 (s), 1478 (w), 1440 (m), 1374 (w), 1245 (s), 1213 (s), 1198 (w), 1168 (w), 1157 (s), 1102 (w), 1015 (w), 837 (s), 815 (w), 839 (s), 734 (w). ^{19}F NMR (672 MHz, $CDCl_3$): δ −57.06, −116.83, −118.12. Anal. calc. for $C_{50}H_{38}Cl_2FeF_7N_3O$ (956.61): C, 62.78; H, 4.00; N, 4.39. Found: C, 62.54; H, 4.28; N, 4.63.

Ar = 2,6-Et$_2$C$_6$H$_3$ (**Fe2**): By employing a methodology analogous to that detailed for **Fe1**, with molar ratios similarly adjusted, but utilizing **L2** in lieu of **L1**, **Fe2** was synthesized and isolated as a blue powder (0.19 g, 73%). FT-IR (cm^{-1}): 3067 (w), 2968 (w), 2931 (w), 1600 (C═N, m), 1506 (s), 1447 (m), 1372 (w), 1253 (w), 1221 (m), 1159 (s), 1198 (w), 1099 (w), 1015 (w), 1102 (w), 836 (s), 656 (w). ^{19}F NMR (672 MHz, $CDCl_3$): δ −56.95, −116.37, −117.02. Anal. calc. for $C_{52}H_{42}Cl_2FeF_7N_3O$ (984.66): C, 63.43; H, 4.30; N, 4.27. Found: C, 63.51; H, 4.53; N, 4.55.

Ar = 2,6-i-Pr$_2$C$_6$H$_3$ (**Fe3**): By employing a methodology analogous to that detailed for **Fe1**, with molar ratios similarly adjusted, but utilizing **L3** in lieu of **L1**, **Fe3** was synthesized and isolated as a blue powder (0.23 g, 85%). FT-IR (cm^{-1}): 3064 (w), 2965 (w), 2871 (w), 2161 (w), 1600 (C═N, w), 1581 (w), 1505 (vs), 1445 (w), 1370 (w), 1321 (w), 1250 (w), 1227 (w), 1205 (w), 1167 (w), 1158 (m), 1098 (w), 1014 (w), 875 (w), 836 (m), 820 (w), 789 (w), 770 (w), 733 (w), 712 (w). ^{19}F NMR (672 MHz, $CDCl_3$): δ −54.64, −114.66, −115.90. Anal. calc. for $C_{51}H_{46}Cl_2FeF_7N_3O$ (1012.72): C, 64.05; H, 4.58; N, 4.15. Found: C, 63.82; H, 4.61; N, 4.39.

Ar = 2,4,6-Me$_3$C$_6$H$_2$ (**Fe4**): By employing a methodology analogous to that detailed for **Fe1**, with molar ratios similarly adjusted, but utilizing **L4** in lieu of **L1**, **Fe4** was synthesized and isolated as a blue powder (0.21 g, 80%). FT-IR (cm^{-1}): 2930 (w), 2962 (w), 1642 (w), 1602 (C═N, m), 1505 (s), 1439 (w), 1374 (w), 1248 (m), 1216 (m), 1178 (w), 1158 (w), 1094 (w), 1014 (w), 867 (w), 837 (w), 818 (w), 786 (w), 655 (w). ^{19}F NMR (672 MHz, $CDCl_3$): δ −57.06, −116.33, −117.06. Anal. calc. for $C_{51}H_{40}Cl_2FeF_7N_3O$ (970.63): C, 63.11; H, 4.15; N, 4.33. Found: C, 63.00; H, 4.20; N, 4.35.

Ar = 2,6-Et$_2$-4-MeC$_6$H$_2$ (**Fe5**): By employing a methodology analogous to that detailed for **Fe1**, with molar ratios similarly adjusted, but utilizing **L5** in lieu of **L1**, **Fe5** was synthesized and isolated as a blue powder (0.19 g, 73%). FT-IR (cm^{-1}): 2930 (w), 2962 (w), 1642 (w), 1602 (C═N, m), 1505 (s), 1439 (w), 1374 (w), 1248 (m), 1216 (m), 1178 (w), 1158 (w), 1094 (w), 1014 (w), 867 (w), 837 (w), 818 (w), 786 (w), 655 (w). ^{19}F NMR (672 MHz, $CDCl_3$): δ −57.06, −116.33, −117.06. Anal. calc. for $C_{53}H_{44}Cl_2FeF_7N_3O$ (998.69): C, 63.74; H, 4.44; N, 4.21. Found: C, 63.58; H, 4.43; N, 4.37.

Ar = 2,6-(4-FPh)$_2$-4-OCF$_3$C$_6$H$_2$ (**Fe6**): By employing a methodology analogous to that detailed for **Fe1**, with molar ratios similarly adjusted, but utilizing **L6** in lieu of **L1**, **Fe6** was synthesized and isolated as a blue powder (0.31 g, 81%). FT-IR (cm^{-1}): 2930 (w), 2962 (w), 1642 (w), 1602 (C═N, m), 1505 (s), 1439 (w), 1374 (w), 1248 (m), 1216 (m), 1178 (w), 1158 (w), 1094 (w), 1014 (w), 867 (w), 837 (w), 818 (w), 786 (w), 655 (w). ^{19}F NMR (672 MHz, $CDCl_3$): δ −56.28, −114.21, −114.94. Anal. calc. for $C_{75}H_{49}Cl_2FeF_{14}N_3O_2$ (1416.96): C, 63.57; H, 3.49; N, 2.97. Found: C, 63.51; H, 3.53; N, 3.05.

X-ray diffraction studies

Single crystals of **Fe4** and **Fe6**, suitable for X-ray diffraction analysis, were grown through the slow diffusion of diethyl ether into their respective dichloromethane solutions at room temperature, all under a nitrogen atmosphere to ensure an inert environment. A crystal of optimal quality from each compound was carefully selected and mounted onto an XtaLAB Synergy R, HyPix diffractometer, which featured a graphite-monochromated Cu-Kα radiation source (λ = 1.54184 Å) and a nitrogen cold stream for temperature control. Throughout the data collection process, the crystals were maintained at a precise temperature of 169.98(10) K to minimize thermal effects on the diffraction patterns. Utilizing the Olex2 software suite,[20] the crystal structures were solved by employing the ShelXT[21] structure solution program, which leveraged intrinsic phasing techniques. Following the initial solution, the structures were refined using the ShelXL[22] refinement package, which applied least-squares minimization to optimize the structural parameters. During the structural refinement, the disordered solvent in the cell structure was squeezed (**Fe6**) with PLATON software.[23] The comprehensive details of the X-ray structure determinations and refinement processes are documented in Table S1.† In the case of **Fe4**, twinned crystals were obtained, and resolving the twinning proved challenging. Nevertheless, the data obtained fully support the proposed structure.

General methods for ethylene polymerization

Ethylene polymerization at ethylene pressures of 5 or 10 atm. The polymerization reactions conducted at ethylene pressures ($P_{C_2H_4}$) of either 5 or 10 atm were executed within a 250 mL stainless-steel autoclave, which was furnished with a mechanical stirrer, along with sophisticated systems for pressure and temperature control. Prior to the experiment, the autoclave was meticulously dried and subsequently evacuated

under vacuum. It was then purged twice with nitrogen and once with ethylene to ensure an inert atmosphere. Upon attainment of the desired temperature, a solution comprising the iron pre-catalyst dissolved in toluene or hexane (50 mL) was injected into the autoclave, immediately followed by an additional 25 mL of toluene or hexane. Subsequently, the requisite quantity of aluminum activator (either MAO or MMAO) was introduced, and a further 25 mL of toluene or hexane was injected using a syringe to finalize the addition process. The autoclave was promptly pressurized to the specified ethylene pressure and vigorously agitated at a speed of 400 revolutions per minute. Following the completion of the predetermined reaction duration, the ethylene pressure was safely released, and the reaction mixture was quenched using a solution of 10% hydrochloric acid in ethanol. Ethanol was employed to precipitate and collect the resulting polymer. Subsequently, the obtained polymer was thoroughly washed with ethanol, dried under reduced pressure at 100 °C, and then weighed for further analysis.

Ethylene polymerization at an ethylene pressure of 1 atm

For the polymerization reactions conducted at an ethylene pressure ($P_{C_2H_4}$) of 1 atm, the co-catalyst was first introduced into a dry Schlenk vessel, which was equipped with a stir bar. The vessel was then evacuated to create a vacuum and subsequently backfilled with ethylene. Freshly distilled toluene (30 mL) was introduced into the vessel, followed by the necessary amount of activator (either MAO or MMAO). The reaction mixture was stirred under an ethylene pressure of 1 atm for a duration of 30 minutes. Once the stirring period was complete, the ethylene supply was terminated, and the pressure was vented from the vessel. The reaction mixture was then quenched using a solution of 10% hydrochloric acid in ethanol. The resulting polymer was collected by precipitation, washed with ethanol, and finally dried under reduced pressure at 100 °C for further use or analysis.

Conclusions

A series of bis(imino)pyridine iron(II) chloride complexes, featuring trifluoromethoxy and difluorobenzhydryl moieties, was synthesized, thoroughly characterized and systematically evaluated as precatalysts for ethylene polymerization. Upon activation with methylaluminoxane (MAO) or modified methylaluminoxane (MMAO), these iron complexes exhibit exceptionally high catalytic proficiency and remarkable thermal stability during ethylene polymerization, producing highly linear polyethylenes with predominantly vinyl-terminated groups, suitable for applications in the production of functional polymers, coatings and lubricant additives. Notably, when MAO-activated, **Fe1** demonstrated peak catalytic activity, achieving a level of 17.28×10^6 g (PE) mol^{-1} (Fe) h^{-1} at 70 °C in hexane. The molecular weight of the resultant PE ranged from 2.0 to 567.7 kg mol^{-1}, adjustable through modifications in the ligand structure (**Fe1–Fe6**) or alterations in the polymerization conditions. Intriguingly, sterically hindered complexes, such as **Fe6** and **Fe3**, generated PEs with elevated molecular weights, underscoring the beneficial influence of bulkier substituents on chain propagation processes. Furthermore, the incorporation of remote fluoro groups and trifluoromethoxy substituents was found to positively impact both catalytic performance and thermal stability, aligning with our prior research findings. Notably, superior catalytic performance was achieved in hexane, a solvent of significant industrial relevance, highlighting the potential of these iron complexes for practical, industrial applications.

Author contributions

Hosseinzadeh Z., Zhang Q., and Sun W.-H. made substantial contributions to the conception and design of the study and performed data analysis and interpretation; Wang Y., Wang Q., Ren G., Liang T., and Ma Y performed data acquisition and provided administrative, technical, and material support.

Conflicts of interest

All authors declared that there are no conflicts of interest.

Data availability

The data supporting this article have been included as part of the ESI.†

Acknowledgements

Z. H. is grateful to the Chinese Academy of Sciences President's International Fellowship Initiative (no. 2020PM0055).

References

1 (*a*) J. Zheng, Y. Zhang, D. Hou, Y. Qin, W. Guo, C. Zhang and J. Shi, *Front. Mech. Eng.*, 2018, **13**, 535–545; (*b*) M. Jacobs and J. Van Dingenen, *J. Mater. Sci.*, 2001, **36**, 3137–3142.
2 E. I. Negishi, *Angew. Chem., Int. Ed.*, 2011, **50**, 6738–6764.
3 (*a*) G. Natta, P. Pino, P. Corradini, F. Danusso, E. Mantica, G. Mazzanti and G. Moraglio, *J. Am. Chem. Soc.*, 1955, **77**, 1708–1710; (*b*) M. Stürzel, S. Mihan and R. Mülhaupt, *Chem. Rev.*, 2016, **116**, 1398–1433; (*c*) M. Delferro and T. J. Marks, *Chem. Rev.*, 2011, **111**, 2450–2485; (*d*) W. Kaminsky, *Polyolefins: 50 Years After Ziegler and Natta II*, Springer, Berlin, 2013; (*e*) P. E. Figgins and D. H. Busch, *J. Am. Chem. Soc.*, 1960, **82**, 820–824; (*f*) G. J. Britovsek, V. C. Gibson and D. F. Wass, *Angew. Chem., Int. Ed.*, 1999, **38**, 428–447.

4 (*a*) B. L. Small, M. Brookhart and A. M. Bennett, *J. Am. Chem. Soc.*, 1998, **120**, 4049–4050; (*b*) G. P. Britovsek, V. Gibson, S. McTavish, G. Solan, A. P. White, D. Williams, B. Kimberley and P. Maddox, *Chem. Commun.*, 1998, **7**, 849–850; (*c*) G. J. Britovsek, M. Bruce, V. C. Gibson, B. S. Kimberley, P. J. Maddox, S. Mastroianni, S. J. McTavish, C. Redshaw, G. Solan and S. Strömberg, *J. Am. Chem. Soc.*, 1999, **121**, 8728–8740; (*d*) W.-H. Sun, S. Jie, S. Zhang, W. Zhang, Y. Song, H. Ma, J. Chen, K. Wedeking and R. Fröhlich, *Organometallics*, 2006, **25**, 666–677; (*e*) D. Takeuchi, S. Takano, Y. Takeuchi and K. Osakada, *Organometallics*, 2014, **33**, 5316–5323.

5 (*a*) Z. Wang, G. A. Solan, W. Zhang and W.-H. Sun, *Coord. Chem. Rev.*, 2018, **363**, 92–108; (*b*) S.-F. Yuan, Y. Yan, G. A. Solan, Y. Ma and W.-H. Sun, *Coord. Chem. Rev.*, 2020, **411**, 213254; (*c*) A. M. F. Phillips, H. Suo, F. C. Maria, A. J. Pombeiro and W.-H. Sun, *Coord. Chem. Rev.*, 2020, **416**, 213332; (*d*) H. Suo, G. A. Solan, Y. Ma and W.-H. Sun, *Coord. Chem. Rev.*, 2018, **372**, 101–116; (*e*) Y. Wang, W. Zhang, X. Wang, Y. Ma and W.-H. Sun, *Acta Polym. Sin.*, 2023, **54**, 564–583.

6 (*a*) J. Yu, H. Liu, W. Zhang, X. Hao and W.-H. Sun, *Chem. Commun.*, 2011, **47**, 3257–3259; (*b*) M. Liu, Z. Ning, Y. Ma, G. A. Solan, T. Liang and W.-H. Sun, *J. Organomet. Chem.*, 2023, **994**, 122740; (*c*) Q. Mahmood, J. Guo, W. Zhang, Y. Ma, T. Liang and W.-H. Sun, *Organometallics*, 2018, **37**, 957–970; (*d*) X. Cao, F. He, W. Zhao, Z. Cai, X. Hao, T. Shiono, C. Redshaw and W.-H. Sun, *Polymer*, 2012, **53**, 1870–1880; (*e*) Q. Mahmood, E. Yue, J. Guo, W. Zhang, Y. Ma, X. Hao and W.-H. Sun, *Polymer*, 2018, **159**, 124–137; (*f*) T. Liu, Y. Ma, G. A. Solan, T. Liang and W.-H. Sun, *Appl. Organomet. Chem.*, 2021, **35**, e6259.

7 (*a*) W.-H. Sun, W. Zhao, J. Yu, W. Zhang, X. Hao and C. Redshaw, *Macromol. Chem. Phys.*, 2012, **213**, 1266–1273; (*b*) T. Liu, Y. Ma, A. S. Solan, Y. Sun and W.-H. Sun, *New J. Chem.*, 2023, **47**, 5786–5795; (*c*) T. Liu, Y. Ma, G. Solan, T. Liang and W.-H. Sun, *Appl. Organomet. Chem.*, 2021, **35**, e6259; (*d*) R. Zhang, M. Han, Y. Ma, G. A. Solan, T. Liang and W.-H. Sun, *Dalton Trans.*, 2019, **48**, 17488–17498.

8 Z. Hosseinzadeh, Q. Zhang, Q. Wang, A. M. Ashfaq, T. Liang, Y. Ma and W.-H. Sun, *ChemPlusChem*, 2025, **90**, e202500007.

9 (*a*) E. Castagnetti and M. Schlosser, *Chem. – Eur. J.*, 2002, **8**, 799–804; (*b*) F. R. Leroux, B. Manteau, J.-P. Vors and S. Pazenok, *Beilstein J. Org. Chem.*, 2008, **4**, 13.

10 J. Lai, W. Zhao, W. Yang, C. Redshaw, T. Liang, Y. Liu and W.-H. Sun, *Polym. Chem.*, 2012, **3**, 787–793.

11 (*a*) T. M. Smit, A. K. Tomov, G. J. Britovsek, V. C. Gibson, A. J. White and D. J. Williams, *Catal. Sci. Technol.*, 2012, **2**, 643–655; (*b*) S. Wang, B. Li, T. Liang, C. Redshaw, Y. Li and W.-H. Sun, *Dalton Trans.*, 2013, **42**, 9188–9197; (*c*) W. Zhao, E. Yue, X. Wang, W. Yang, Y. Chen, X. Hao, X. Cao and W.-H. Sun, *J. Polym. Sci., Part A: Polym. Chem.*, 2017, **55**, 988–996; (*d*) N. V. Semikolenova, W.-H. Sun, I. E. Soshnikov, M. A. Matsko, O. V. Kolesova, V. A. Zakharov and K. P. Bryliakov, *ACS Catal.*, 2017, **7**, 2868–2877; (*e*) D. P. Gates, S. A. Svejda, E. Oñate, C. M. Killian, L. K. Johnson, P. S. White and M. Brookhart, *Macromolecules*, 2000, **33**, 2320–2334; (*f*) C. S. Popeney, A. L. Rheingold and Z. Guan, *Organometallics*, 2009, **28**, 4452–4463.

12 (*a*) S. Zhang, I. Vystorop, Z. Tang and W.-H. Sun, *Organometallics*, 2007, **26**, 2456–2460; (*b*) S. Zhang, W.-H. Sun, X. Kuang, I. Vystorop and J. Yi, *J. Organomet. Chem.*, 2007, **692**, 5307–5316.

13 (*a*) S. A. Cantalupo, H. E. Ferreira, E. Bataineh, A. J. King, M. V. Petersen, T. Wojtasiewicz, A. G. DiPasquale, A. L. Rheingold and L. H. Doerrer, *Inorg. Chem.*, 2011, **50**, 6584–6596; (*b*) J. Yuan, W.-B. Shi and H.-Z. Kou, *Transition Met. Chem.*, 2015, **40**, 807–811; (*c*) C. Huang, Y. Zhang, G. A. Solan, Y. Ma, X. Hu, Y. Sun and W.-H. Sun, *Eur. J. Inorg. Chem.*, 2017, **36**, 4158–4166.

14 (*a*) T. Xiao, P. Hao, G. Kehr, X. Hao, G. Erker and W.-H. Sun, *Organometallics*, 2011, **30**, 4847–4853; (*b*) Y. Zhang, C. Huang, X. Hao, X. Hu and W.-H. Sun, *RSC Adv.*, 2016, **6**, 91401–91408; (*c*) V. K. Appukuttan, Y. Liu, B. C. Son, C.-S. Ha, H. Suh and I. Kim, *Organometallics*, 2011, **30**, 2285–2294; (*d*) Q. Mahmood, Y. Zeng, X. Wang, Y. Sun and W.-H. Sun, *Dalton Trans.*, 2017, **46**, 6934–6947.

15 Z. Wang, R. Zhang, W. Zhang, G. A. Solan, Q. Liu, T. Liang and W.-H. Sun, *Catal. Sci. Technol.*, 2019, **9**, 1933–1943.

16 N. E. Mitchell, J. W. C. Anderson and B. K. Long, *J. Polym. Sci., Part A: Polym. Chem.*, 2017, **55**, 3990–3995.

17 (*a*) W.-H. Sun, X. Tang, T. Gao, B. Wu, W. Zhang and H. Ma, *Organometallics*, 2004, **23**, 5037–5047; (*b*) V. C. Gibson, C. Redshaw, G. A. Solan, A. J. White and D. J. Williams, *Organometallics*, 2007, **26**, 5119–5123.

18 W. Zhang, W.-H. Sun and C. Redshaw, *Dalton Trans.*, 2013, **42**, 8988–8997.

19 Z. Hosseinzadeh, M. Liu, Q. Zhang, T. Liang, G. A. Solan, Y. Ma and W.-H. Sun, *Catalysts*, 2022, **12**, 1520.

20 O. V. Dolomanov, L. J. Bourhis, R. J. Gildea, J. A. Howard and H. Puschmann, *J. Appl. Crystallogr.*, 2009, **42**, 339–341.

21 G. M. Sheldrick, *Acta Crystallogr., Sect. A: Found. Adv.*, 2015, **71**, 3–8.

22 G. M. Sheldrick, *Acta Crystallogr., Sect. C: Struct. Chem.*, 2015, **71**, 3–8.

23 L. Spek, *Acta Crystallogr., Sect. D: Biol. Crystallogr.*, 2009, **65**, 148–155.

